Supporting Information

Polarized XANES Monitors Femtosecond Structural Evolution of Photoexcited Vitamin B_{12}

Nicholas A. Miller[1], Aniruddha Deb[1,3], Roberto Alonso-Mori[4], Brady D. Garabato[5], James M. Glownia[4], Laura M. Kiefer[1], Jake Koralek[4], Marcin Sikorski[4], Kenneth G. Spears[1], Theodore E. Wiley[1], Diling Zhu[4], Pawel M. Kozlowski[5,6], Kevin J. Kubarych[1,3], James E. Penner-Hahn[1,3], and Roseanne J. Sension[1,2,3]

[1]Department of Chemistry, University of Michigan, 930 N University Ave. Ann Arbor, Michigan, 48109-1055, USA
[2]Department of Physics, University of Michigan, 450 Church Street, Ann Arbor, Michigan, 48109-1040, USA
[3]Biophysics, University of Michigan, 930 N University Ave. Ann Arbor, Michigan, 48109-1055, USA
[4]Linac Coherent Light Source, SLAC National Accelerator Laboratory, 2575 Sand Hill Road, Menlo Park, CA 94025, USA,
[5]Department of Chemistry, University of Louisville, 2320 South Brook Street, Louisville, Kentucky, 40292, USA
[6]Visiting Professor, Department of Food Sciences, Medical University of Gdansk, Al. Gen J. Hallera, 107, 80-416 Gdansk, Poland

Corresponding Author email: rsension@umich.edu

Contents:

XANES Experimental Methods

Cyanocobalamin from Aldrich was dissolved in ultrapure deionized water to a concentration of 8.8 mM. UV-visible spectra were obtained before and after each set of experiments to ensure sample integrity. These spectra were identical within a scale factor due to a small (10%) increase in concentration from solvent evaporation during the run.

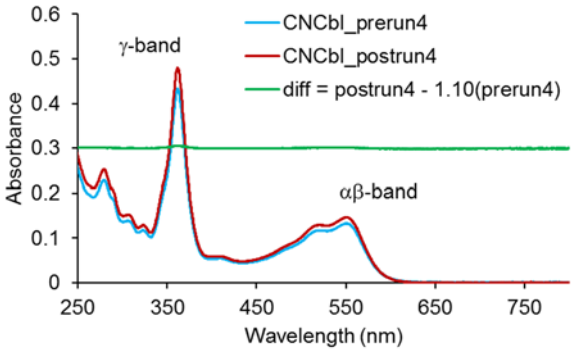

Figure S1. UV-visible absorption spectra of the sample before and after XANES measurements. Aside from a concentration increase due to solvent evaporation the sample is unchanged.

The XANES spectra were collected at the XPP instrument of the LCLS.[1] The sample was placed in a reservoir and pumped through a glass nozzle to achieve a stable 50 μm diameter jet of solution. The x-ray beam and laser beam (550 nm) travel in a nearly collinear geometry (~ 1° crossing angle) and were overlapped with the sample about 500 μm below the nozzle. The XANES spectra were obtained by scanning a Si[111] double-crystal monochromator between 7.7 keV and 7.8 keV (step size = 0.5 eV from 7.7 keV to 7.734 keV and 1 eV from 7.734 keV to 7.8 keV). The FEL energy tracked the monochromator energy setting, the average x-ray flux on the sample were maximized and stayed nearly constant over the whole scanning range that is much larger than the FEL natural bandwidth. However, there is significant pulse energy jitter in the

FEL output after the monochromator such that both the energy and timing of the each pulse could vary significantly. Corrections were applied in the data analysis.[2,3]

Cobalt x-ray absorption was measured as a fluorescence excitation spectrum using two Si diodes (Canberra PIPS A300-17AM), positioned at 90° relative to the laser beams, on each side of the sample in order to minimize the elastic scattering background. The FEL probe operated at 120 Hz while the delay time was alternated at ~60Hz between nominal requested delay and negative delay, thus allowing measurement of alternating light and dark spectra. The monochromator was stepped every 10 seconds giving ~ 400 light and 400 dark measurements for each energy step. The measured XANES spectrum with the optical laser off (Figure S2) is in excellent agreement with the spectrum reported by Champloy et al. for CNCbl free of radiation damage.[4] The use of femtosecond x-ray pulses with a large circulating sample volume avoids the complication of radiation damage. The dark state XANES spectra were compared and found to be identical throughout each run.

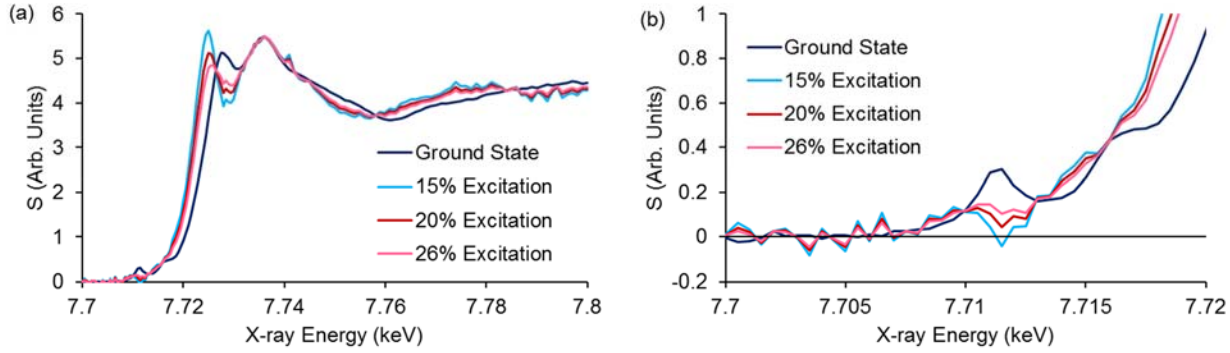

Figure S2. XANES spectra. (a) Measured ground state spectrum (dark blue) and estimated excited state spectra S(C) obtained by adding the given percentage of the ground state spectrum back into the difference spectrum as described below. (b) Expanded view of the pre-edge region.

The measured signal as a function of laser power was used to estimate the percent of the sample excited by the optical pulse. Measurements with a nominal pulse energy of 2, 4, 6, and 8

μJ are compared with a theoretical saturation curve in Figure S3. Because the beam diameter was larger than the sample, the actual energy on the sample can only be estimated. The fraction of molecules in the sample that are excited is estimated from:

$$\text{Fraction Excited} = \frac{\text{Photons Absorbed}}{\text{Total Molecules in Volume}} = \frac{P_{abs}}{N_{Tot}} \tag{S1}$$

and $P_{abs} = P_0\left(1-10^{-\alpha(I)}\right)$ where P_0 is the number of incident photons in the pulse and $\alpha(I)$ is the effective absorption coefficient as a function of incident intensity. The effect absorption coefficient is given by:

$$\alpha(I) = \frac{\alpha_0}{1+I/I_S} \tag{S2}$$

where I_S is a phenomenological saturation intensity. For our measurement the sample concentration was about 8.8 mM, the optical path length was ca. 50 μm, and ε = 8395 M^{-1} cm^{-1} at 550 nm. Given these parameters, $\alpha_0 = 0.369$ in the center of the sample. The saturation intensity is adjusted to give an asymptotic limit of 0.5 for the fraction of molecules excited when the intensity gets high and we expect stimulated emission and absorption to balance. For our parameters, $I_S = 0.508$ μJ.

The best fit of the data to a saturation curve suggests that 20% of the sample was excited when the nominal pulse energy was 4 μJ. This is reasonable based on the absorbance of the sample and the relative sizes of the laser beam and the sample jet. Polarized XANES spectra were obtained using 2 μJ excitation and 4 μJ excitation. Aside from a scale factor reflecting the different population of the excited state, the difference spectra are identical with each other within the measurement signal-to-noise ratio.

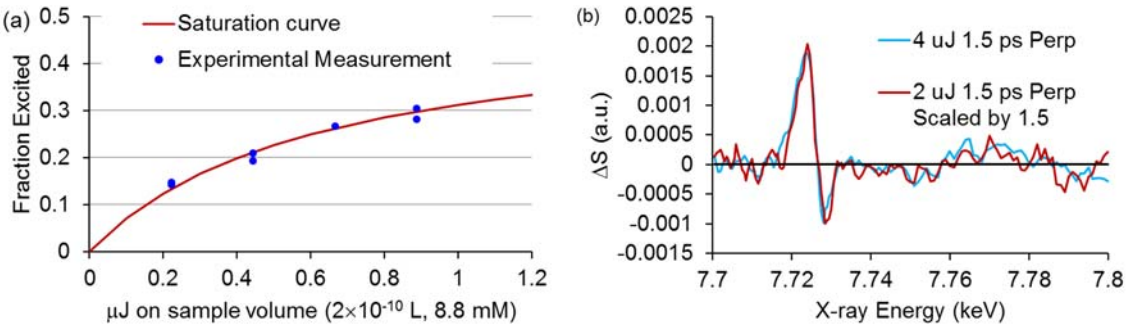

Figure S3. Left: Laser saturation measurement using pulses with nominal energies from 2 μJ to 8 μJ. Only about 10% of the beam interacted with the sample. The saturation curve was calculated as described in the text. Right: Comparison of the difference signal obtained with 2 μJ and 4 μJ excitation pulses.

The excited state XANES spectrum $S(C)$ is estimated by adding the appropriate amount of the ground state spectrum to the measured difference spectrum:

$$S(C) = \frac{1}{\left(\beta \cdot e^{-t/\tau}\right)}\left(S_{On}(t) - S_{Off} + \left(\beta \cdot e^{-t/\tau}\right)S_{off}\right) \tag{S3}$$

where β is the fraction of molecules initially excited, $e^{-t/\tau}$ accounts for population decay prior to the time delay of the measurement, and the pre-factor scales the spectrum to 100% population for comparison with the ground state spectrum and with calculation.

The excitation percentage is greater than 15% as lower percentages leave an unphysical negative signal in the pre-edge region. The saturation behavior sets an upper limit of 26% excitation. The derived excited state spectra for these excitation percentages are also plotted in Figure S2.

UV-Visible Transient Absorption Methods and Analysis:

Transient absorption measurements with 550 nm excitation and a broadband continuum probe spanning the range from 280 nm to 600 nm were performed for comparison with the XANES measurements. The continuum was generated by focusing the 400 nm second harmonic of a

Ti:Sapphire laser into a translating CaF_2 window as described previously.[5] The 550 nm pump pulse was generated using a noncollinear optical parametric amplifier pumped by the same Ti:Sapphire laser. Pump scatter limits useful analysis of the difference spectrum to the range between 280 nm and 530 nm. The sample was a flat wire-guided flow of a 0.43 mM solution of CNCbl in water. The instrument response function modeled as a Gaussian is ~160 fs FWHM. The pump and probe polarizations were set at the magic angle (54.7°) to eliminate any orientation dependence in the data.

The data was analyzed using the freely available global analysis program Glotaran.[6] The data was fit to a sum of three exponential decay components with four amplitudes at each wavelength and three rate constants fit globally to the entire data set.

$$I(\lambda,t) = A_1(\lambda)e^{-k_1 t} + A_2(\lambda)e^{-k_2 t} + A_3(\lambda)e^{-k_3 t} + A_4(\lambda) \quad \text{(S4)}$$

The fit to the data gives rate constants k_1 = 8.9 ps^{-1} (0.11 ± 0.03 ps), k_2 = 3.9 ps^{-1} (0.26 ± 0.03 ps), and k_3 = 0.162 ps^{-1} (6.2 ± 0.1 ps) and the associated amplitudes. The error bars are estimated from multiple fits to the data using different initial conditions and from errors returned by the fitting program (generally smaller than the deviations between fits). The fit is summarized at several time delays and several wavelengths in Figure S4.

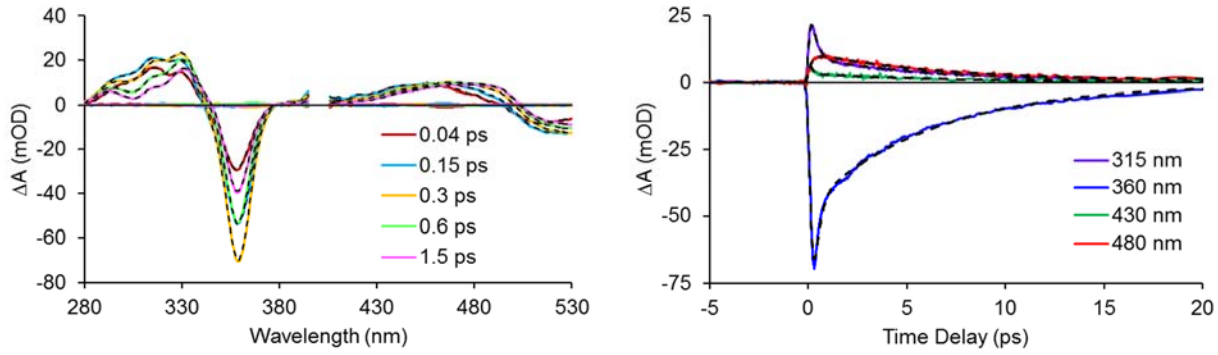

Figure S4. Left: Transient difference spectra obtained following excitation of CNCbl at 550 nm. The 0.15 ps and 0.6 ps spectra fall on top of each other in the region of the γ-

band bleach around 360 nm but are very different at shorter wavelengths. The black dashed lines represent the fits to the data. Right: Transient absorption signal as a function of time at select wavelengths. Again the black dashed lines represent the fits.

The transient XANES spectra probe the very early time dynamics of electronically excited CNCbl. Interpretation of these data are facilitated by comparison with the UV-Visible data. The very early time dynamics in the UV-visible transient absorption data are illustrated in Figure S5.

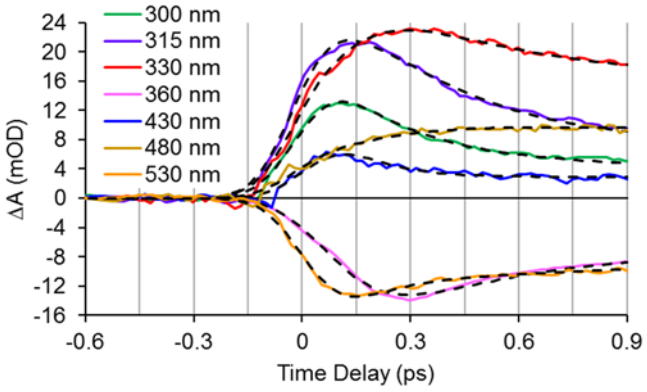

Figure S5. Transient data obtained at seven wavelengths compared with the fit to the data. The γ-band bleach at 360 nm is divided by 5 to fit on a comparable scale.

The presence of several time-dependent contributions to the signal is apparent in this data. The bleach of the γ-band at 360 nm and the absorption at 330 nm reach a maximum at ~300 fs while the peak of the signal comes at about 150 fs at 315 nm and 530 nm and somewhat earlier at 300 nm and 430 nm. In contrast the signal at 480 nm grows in on an even longer time scale corresponding to the decay of the 315 nm trace.

Assuming a sequential model: $S_0 \xrightarrow{h\nu} S_A \xrightarrow{k_1} S_B \xrightarrow{k_2} S_C \xrightarrow{k_3} S_0$, the population of the excited states are obtained from the fit to the data by solving the coupled differential equations:

$$\begin{aligned}
\dot{n}_{S_A}(t) &= -k_1\, n_{S_A}(t) \\
\dot{n}_{S_B}(t) &= k_1\, n_{S_A}(t) - k_2\, n_{S_B}(t) \\
\dot{n}_{S_C}(t) &= k_2\, n_{S_B}(t) - k_3\, n_{S_C}(t) \\
\dot{n}_{S_0}(t) &= k_3 n_{S_C}(t)
\end{aligned} \tag{S5}$$

Considering only the population excited by a delta function optical pump pulse so that the initial population of S_A, $n_{S_A}(0) = 1$, the populations are given by:

$$\begin{aligned}
n_{S_A}(t) &= e^{-k_1 t} \\
n_{S_B}(t) &= \frac{k_1}{k_1 - k_2}\left(e^{-k_2 t} - e^{-k_1 t}\right) \\
n_{S_C}(t) &= k_1 k_2 \left(\frac{e^{-k_1 t}}{(k_1 - k_2)(k_1 - k_3)} + \frac{e^{-k_2 t}}{(k_2 - k_1)(k_2 - k_3)} + \frac{e^{-k_3 t}}{(k_3 - k_1)(k_3 - k_2)} \right) \\
n_{S_0}(t) &= 1 - \left(\frac{k_2 k_3 e^{-k_1 t}}{(k_1 - k_2)(k_1 - k_3)} + \frac{k_1 k_3 e^{-k_2 t}}{(k_2 - k_1)(k_2 - k_3)} + \frac{k_1 k_2 e^{-k_3 t}}{(k_3 - k_1)(k_3 - k_2)} \right)
\end{aligned} \tag{S6}$$

The transient absorption signal can be given in terms of the difference spectrum for each species.

$$I(\lambda, t) = \Delta A_{S_A}(\lambda)\, n_{S_A}(t) + \Delta A_{S_B}(\lambda)\, n_{S_B}(t) + \Delta A_{S_C}(\lambda)\, n_{S_C}(t) + \Delta A_{S_0}(\lambda)\, n_{S_0}(t) \tag{S7}$$

Collecting terms for each exponential component the species associated difference spectra (SADS) are given by:

$$\begin{aligned}
\Delta A_{S_A}(\lambda) &= A_1(\lambda) + A_2(\lambda) + A_3(\lambda) + A_4(\lambda) \\
\Delta A_{S_B}(\lambda) &= \frac{(k_1 - k_2)}{k_1} A_2(\lambda) + \frac{(k_1 - k_3)}{k_1} A_3(\lambda) + A_4(\lambda) \\
\Delta A_{S_C}(\lambda) &= \frac{(k_2 - k_3)(k_1 - k_3)}{k_1 k_2} A_3(\lambda) + A_4(\lambda) \\
\Delta A_{S_0}(\lambda) &= A_4(\lambda) \approx 0
\end{aligned} \tag{S8}$$

The finite lifetime of the excitation pulse is taken into account by convoluting the signal with a Gaussian instrument response function when fitting the data.

The decay associated difference spectra (DADS) plotted directly from the fitted amplitudes of each time component vs. wavelength and the computed species associated difference spectra (SADS) obtained from the fitted parameters and the consecutive kinetic model are plotted in Figure S6.

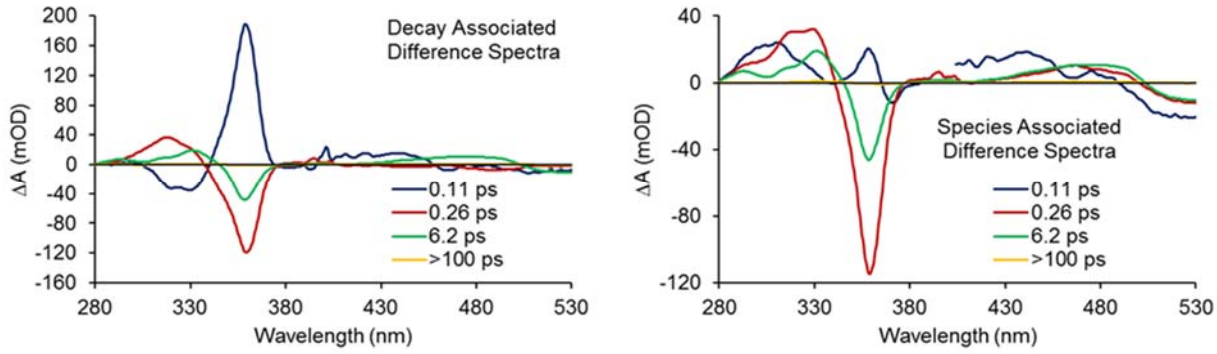

Figure S6. Decay associated and species associated difference spectra obtained from the fit to the transient absorption data.

The short-lived excited state produced by the optical pulse is characterized by an increase in the intensity of the γ-band and small changes across the rest of the spectrum. The instrument response function for the measurement (~160 fs) is longer than the lifetime of the short component and this introduces uncertainty into the precise rate constant and thus the amplitudes derived from the fit. Nonetheless it is clear that a fast component is required by the data and that this corresponds to an increased absorption at 315 nm and 430 nm and a stronger γ-band absorption at 360 nm than either of the two later states.

The 260 fs species is characterized primarily by a reduction in the intensity of the γ-band and an increase in the intensity at shorter wavelengths. The αβ-band also shifts to shorter wavelength. The S_1 state decaying on a 6 ps time scale has a spectrum consistent with those

reported earlier exhibiting a blue shift αβ-band and a decrease in the intensity of the γ-band compared with the ground state. Fits to the kinetic traces illustrating the contributions from each species are plotted in Figure S7.

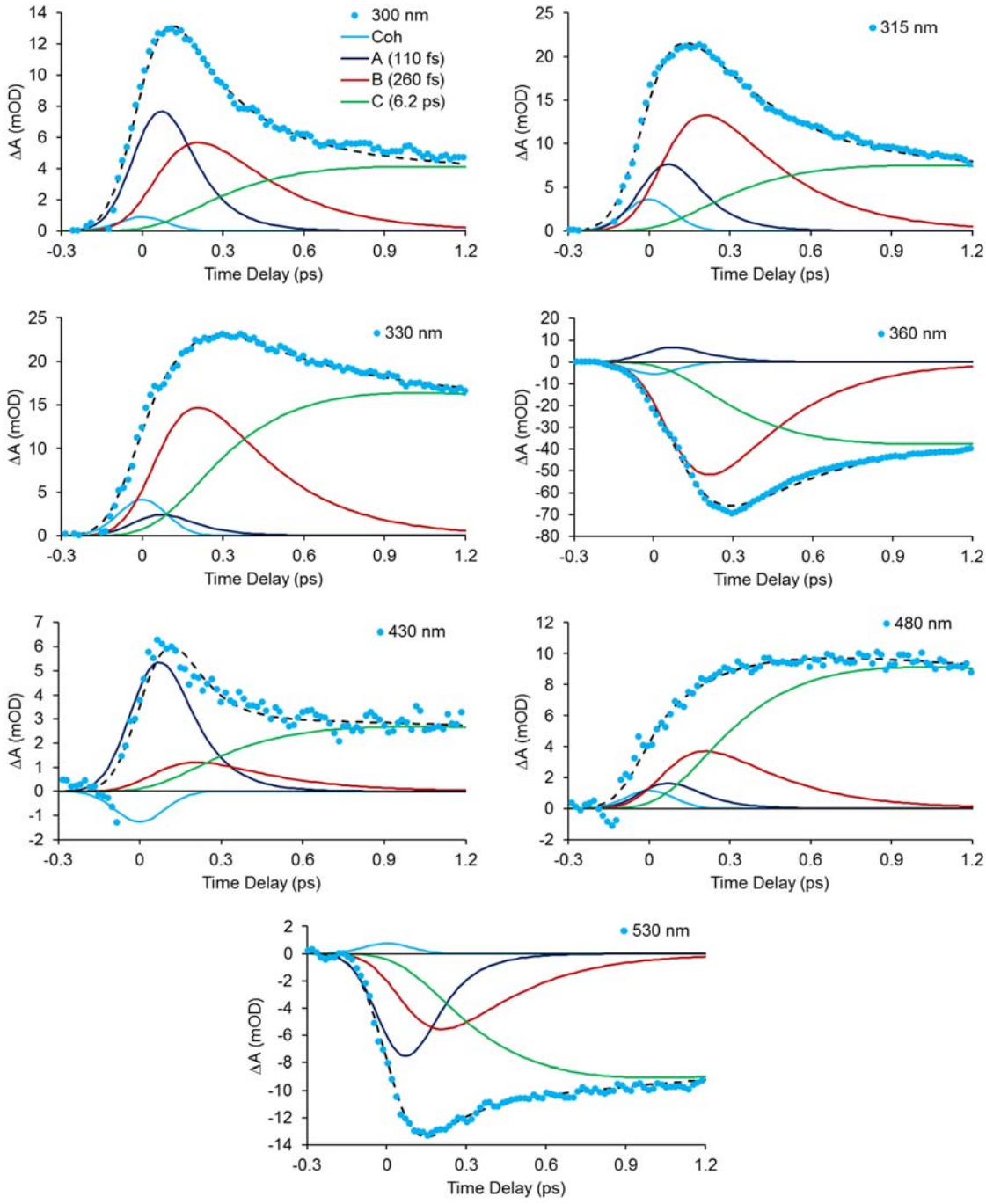

Figure S7. Fits to the kinetic traces at select wavelengths illustrating the population dynamics of the three species identified in the global fit of the data. The light blue solid line is an instrument limited coherent contribution. The other three components correspond to the species in the SADS. The colors match those in Figure S6.

Time-Dependent XANES Data

Kinetic traces at 7.723 and 7.725 keV were measured for perpendicular polarization by sitting at the desired x-ray energy and scanning the time delay between the x-ray pulse and the laser pulse. This temporal behavior of these traces is in excellent agreement with the rate constants determined from the transient absorption data as illustrated in Figure S8. In the plot the time constants were held to those obtained from the UV-visible data and only the amplitudes were varied.

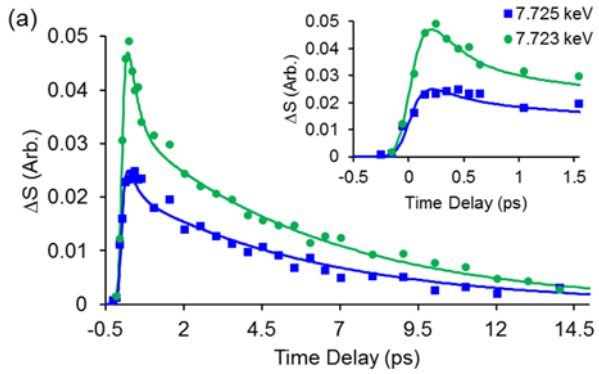

Figure S8. XAS difference signal for laser-on and laser-off as a function of time delay at two x-ray energies near the peak of the signal. The line is a fit to the data using the kinetic components determined for the UV-Visible transient absorption with the only the amplitudes allowed to vary.

The jitter of x-ray/laser synchronization was used to obtain time-resolved XANES spectra for parallel and perpendicular polarization for time delays from -150 fs to 700 fs. The data was analyzed using 50 fs bins centered every 25 fs. The temporal behavior centered at select x-ray energies is illustrated in the left-hand panel of figure S9 below. Each trace represents an average over 1 to 4 eV. These traces can be used to construct the time dependence for the contributions

along the *x*-direction parallel to the optical transition dipole moment and the *y*- and *z*-directions perpendicular to the transition dipole moment.

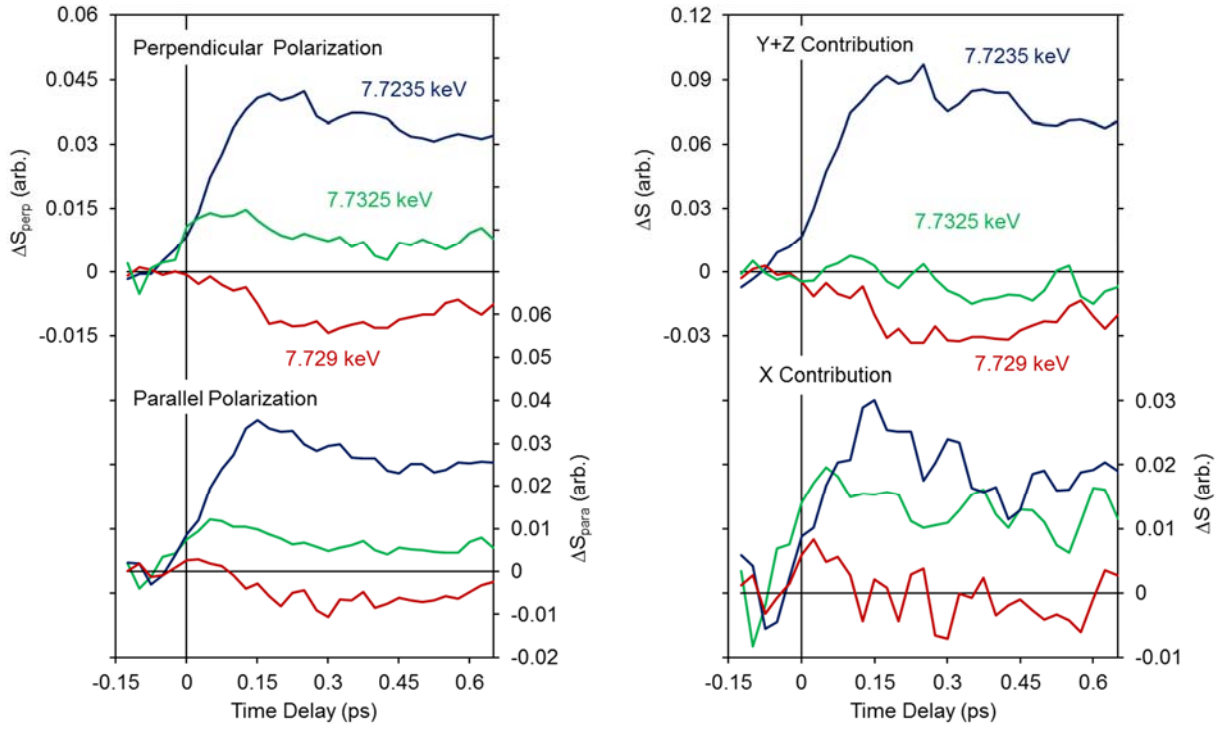

Figure S9. Left: XANES difference signal as a function of time delay for parallel and perpendicular polarization directions at select x-ray energies. Right: *y*+*z* and *x* contributions calculated from the measurements.

There is a clear delay in the rise of the transient signal at some x-ray energies with respect to others. The *x* and *y*+*z* traces at eight x-ray energies were fit to a model consisting of a sum of exponential decay components as in Eq. S4. The instrument response (~70 fs) was modeled as a Gaussian function and convoluted with Eq. S4 in the fits. An exponential model may not capture all the nuance of atomic motion and structural evolution following excitation of CNCbl, but provides a helpful way to characterize the data. The longest time constant is set at 6.2 ps corresponding to the overall decay of the excited state population. The other two time constants were allowed to vary resulting in $\tau_1 = 0.12 \pm 0.03$ ps and $\tau_2 \approx 0.30 \pm 0.1$ ps. These values are in

good agreement with $\tau_1 = 0.11 \pm 0.03$ ps and $\tau_2 = 0.26 \pm 0.03$ ps obtained from the fit to the UV-Visible transient absorption data.

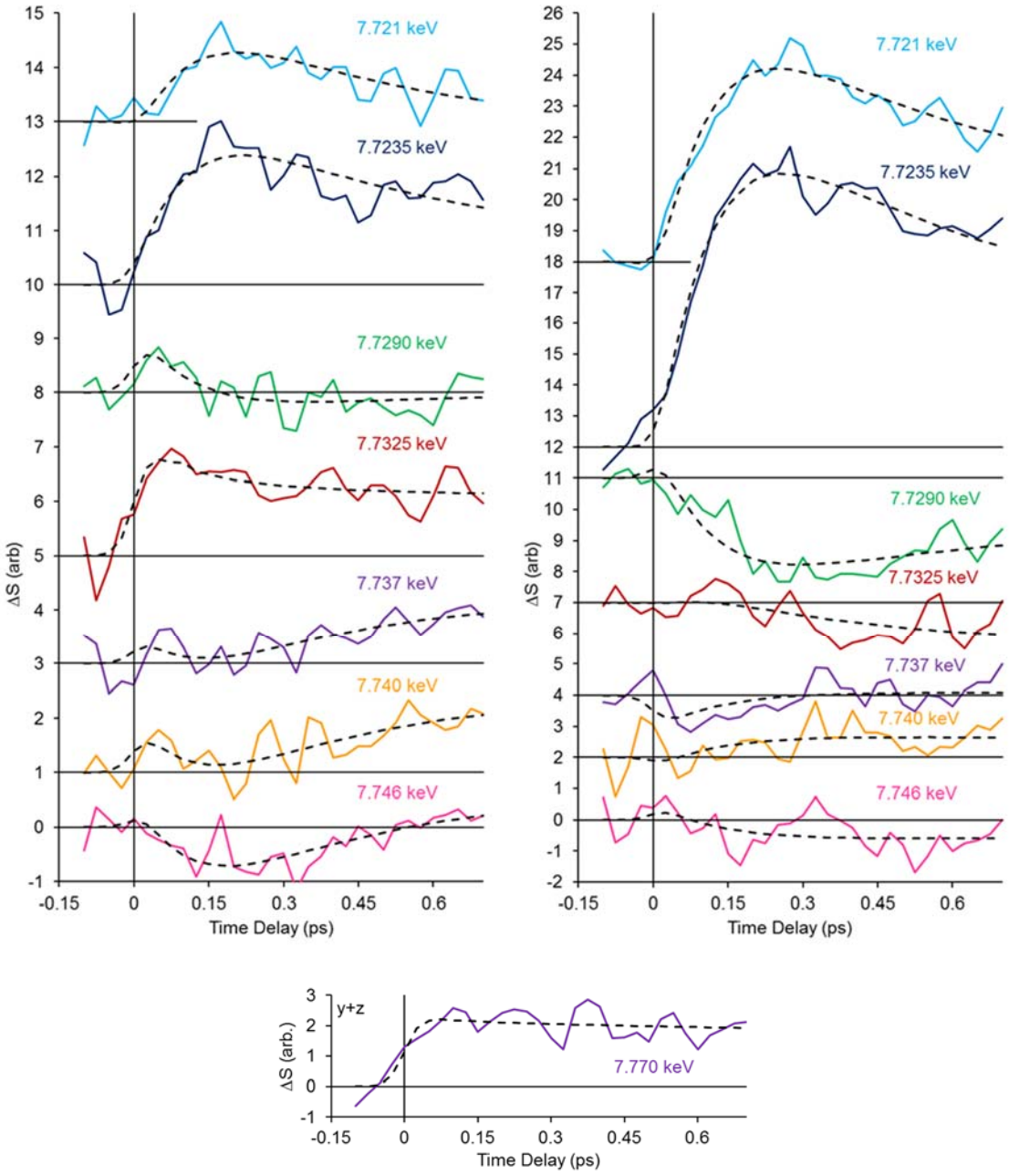

Figure S10. The *x* (left panel) and *y*+*z* (right panel) contributions to the XANES difference spectrum as a function of time at select x-ray energies. The data are fit (black dashed lines) to a model consisting of a sum of exponential components as described in the text. The x component of the 7.770 keV signal is negligible.

Simulated XANES Difference Spectra.

The excited state XANES spectra were simulated using FDMNES (see main text) using the truncated structural model shown in Figure S11. Polarized spectra were calculated along the *x*, *y*, and *z* directions.

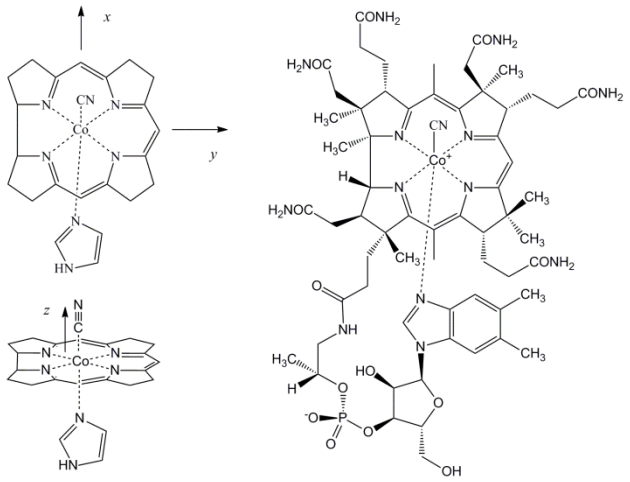

Figure S11. Left: Truncated structure used in most calculations along with a definition of the *x*, *y*, and *z* directions. Right: Full structure of cyanocobalamin.

Ground state DFT calculations have been performed for both the truncated structure (Figure S11, left) and the full cobalamin (Figure S11, right). While the structures are generally quite similar, the presence of the ribose tail in the full structure causes the imidazole to tilt in the full structure; no such constraint is present in the truncated structures. This constraint changes the Co-N-N and Co-N-C angles from 160.5° and 163.5° (truncated calculation) to 155.8° and 168.0° (full calculation), as shown in Figure S12. In addition, some of the calculations with the truncated cobalamin had the imidazole rotated by 180° (see Figure S12).

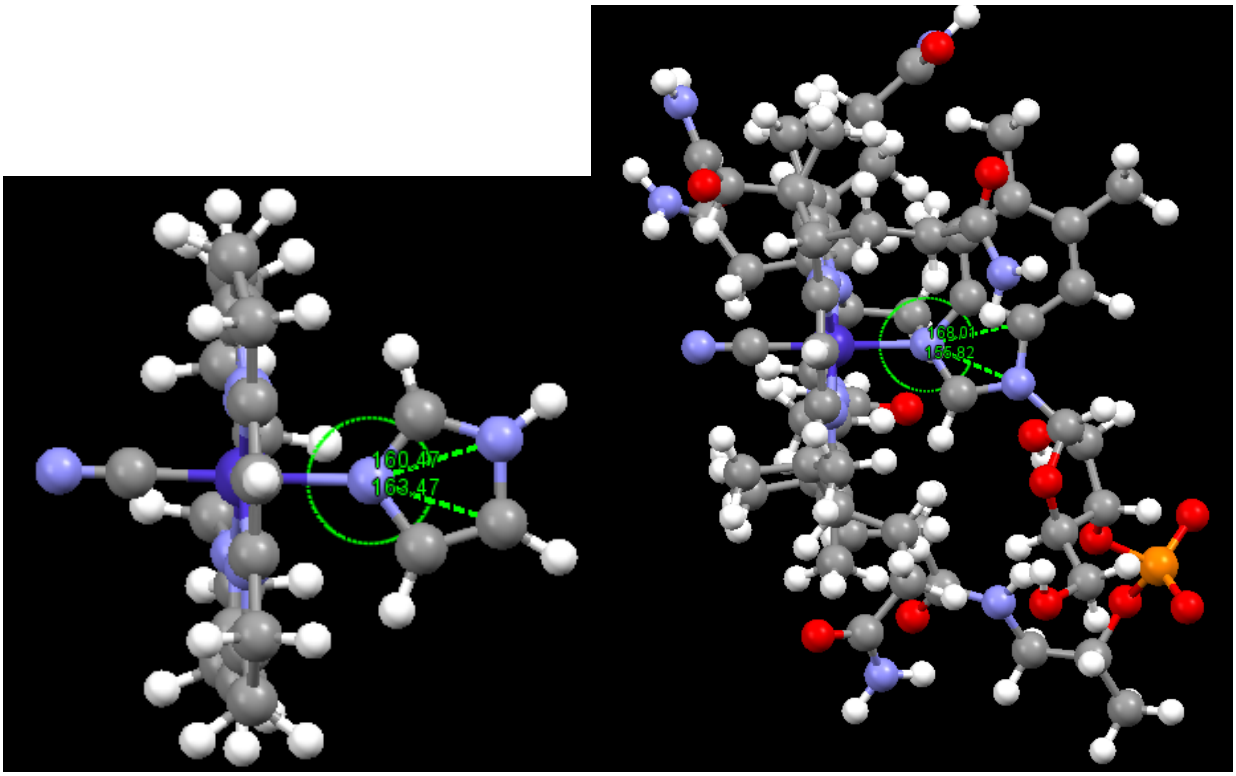

Figure S12. Left: DFT calculation of the ground state for the truncated cobalamin. Right: DFT calculation of the ground state structure for the full cobalamin.

Since XANES spectra are sensitive to multiple scattering, which peaks as the multiple-scattering pathways approach 180°, these small changes in tilt cause a noticeable change in the calculated XANES. For this reason, all XANES simulations started from the full cobalamin calculation (Figure S11, right). The position of the core non-H atoms were taken from the full cobalamin DFT calculation. H positions were calculated by scaling the C-C vectors in the full structure to match the C-H distance in the truncated DFT calculation. Together, these gave the ground-state truncated structure.

Since DFT calculations of the excited state of the full, 181 atom cobalamin are prohibitive, we estimated the excited state structure as follows. For each of the 56 atoms in the truncated

structure, we calculated a vector $\vec{d}_i$ representing the difference in position for atom i between the DFT structures (using a truncated model) for S_0 and S_1C:

$$\vec{d}_i = S_0C_i - S_{0_i} \tag{S9}$$

These vectors were then applied to the truncated ground-state structure (above)

$$S_0C_i' = S_{0_i} + \vec{d}_i \tag{S10}$$

to give an our best estimate of the structure of the excited state.

With the exception of the 1s-3d transitions (at ~7710 eV) all of the x-ray absorbance in our spectra is at energies above the Fermi energy. That is, these are all continuum transitions in which the incident x-ray excites a photoelectron from the 1s orbital. This photoelectron propagates as a p-symmetric wave oriented in the direction of the polarization vector of the x-ray. In this energy region the absorbance, μ, can be factored as $\mu=\mu_0(1+\chi)$ where μ_0 is the atomic-like background absorption and χ is the normalized fine structure which reflects the interaction of the photoelectron with the surrounding atoms.[7] Because of the symmetry of the excited photoelectron, when the x-ray polarization is along the molecular z axis, structural features contribute to χ with a weight of $\cos^2\theta$, where θ is the angle between a structural feature and the z axis.[8] The dependence on θ is incorporated into the simulation program (FDMNES) so that our simulated spectra reflect the XANES that would be observed if we were observing a single cobalamin molecule with the polarization oriented along x, y, or z. The isotropic spectrum is the sum of the x, y, and z contributions.

In order to test the sensitivity of the XANES simulations to the presence of the additional atoms beyond the core, we performed additional XANES calculations using the complete 181 atom structure for the ground state. The differences between the two calculations are small (see

Figure S13), validating use of the truncated structure when investigating the difference between the XANES spectra of the ground and excited state

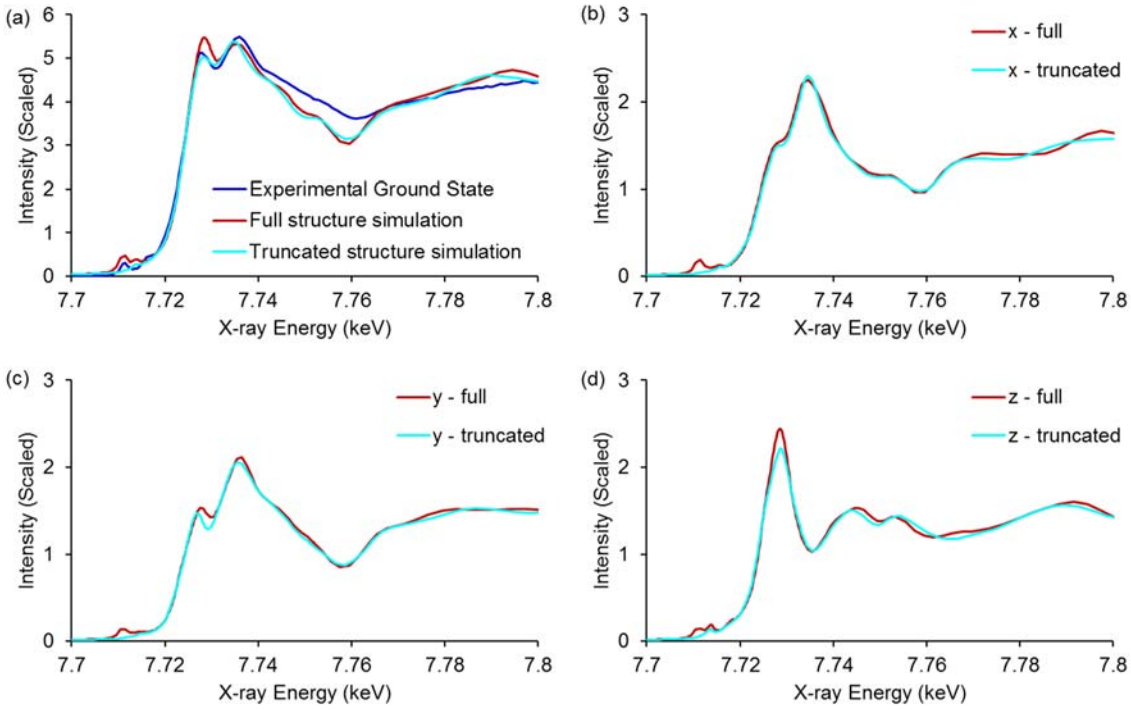

Figure S13. (a) Simulated XANES spectra for the ground using the full and truncated structures compared with the ground state spectrum measured in the present work. The *x*, *y*, and *z*-components of the simulations are compared in (b), (c), and (d). The qualitative features remain the same in all cases, with the largest difference at the peak in the z-direction.

The contributions to the ground and excited state XANES spectra and the difference between the ground and excited state are plotted in Figure S14. The dominant contribution is along the z-direction where the largesgt changes in bond length are predicted.

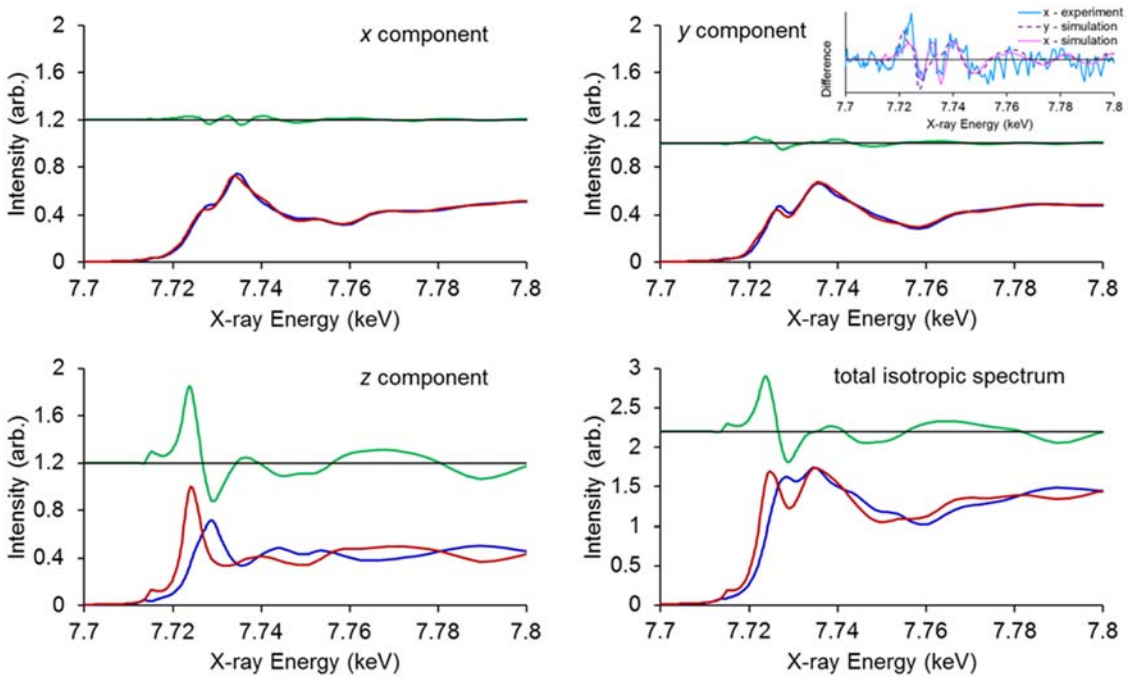

Figure S14. Simulated XANES spectra for the ground and excited state using the truncated structure from [9]. In each panel the blue line is the calculated ground state spectrum, the red line is the calculated excited state spectrum and the green line is the difference between the two, off-set for clarity. The isotropic spectrum is the sum of each of the three directional contributions. The dominant change is in the *z*-direction as observed in the experiments. The *x*- and *y*- components are of similar magnitude. The inset compares the simulated *x*- and *y*- components with the measured difference spectrum in the *x*-direction.

Input files for XANES Simulations

Sample Input:

```
! Indata file for the fdmnes program
! Cncbl K edge in CnCbl_S0A_001
! S0_A state polarization [100], [010], [001]


 Filout
   Sim/Test_stand/xxxxxxx

 Range
-25.  1  0. 0.25 20. 1. 40. 2. 60. 3. 100.
```

```
 Radius
  5.55

Density

SCF

Quadrupole

Edge
K

Polarize
1.0 0.0 0.0  0.0 0.0 1.0
0.0 1.0 0.0  0.0 0.0 1.0
0.0 0.0 1.0  1.0 1.0 0.0


Molecule    ! Description of the molecule (or cluster).

     1    1    1  90  90  90   = a, b, c, alpha, beta, gamma

 cif_file            ! Keyword for reading of a cif file

   Sim/Test_stand/in/xxxx.cif


 End
```

Sample Convolution File

```
   ! Main indata file for fdmnes
   ! Convolution part of the calculation done on CnCbl in a previous
step.

 Calculation
 Sim/Test_stand/xxxxxx.txt

! keywords for the convolution

 Convolution

Efermi
-3.5

Estart
 -16.

Gamma_max
5

Conv_out                  ! To specify an output file name
```

```
    Sim/Test_stand/xxxxxx_conv.txt

End
```

References:

(1) Chollet, M.; Alonso-Mori, R.; Cammarata, M.; Damiani, D.; Defever, J.; Delor, J. T.; Feng, Y. P.; Glownia, J. M.; Langton, J. B.; Nelson, S.; Ramsey, K.; Robert, A.; Sikorski, M.; Song, S.; Stefanescu, D.; Srinivasan, V.; Zhu, D. L.; Lemke, H. T.; Fritz, D. M. *J. Synchrotron Rad.* **2015**, *22*, 503-507.

(2) Minitti, M. P.; Robinson, J. S.; Coffee, R. N.; Edstrom, S.; Gilevich, S.; Glownia, J. M.; Granados, E.; Hering, P.; Hoffmann, M. C.; Miahnahri, A.; Milathianaki, D.; Polzin, W.; Ratner, D.; Tavella, F.; Vetter, S.; Welch, M.; White, W. E.; Fry, A. R. *J. Synchrotron Rad.* **2015**, *22*, 526-531.

(3) Harmand, M.; Coffee, R.; Bionta, M. R.; Chollet, M.; French, D.; Zhu, D.; Fritz, D. M.; Lemke, H. T.; Medvedev, N.; Ziaja, B.; Toleikis, S.; Cammarata, M. *Nature Photonics* **2013**, *7*, 215-218.

(4) Champloy, F.; Gruber, K.; Jogl, G.; Kratky, C. *J. Synchrotron Rad.* **2000**, *7*, 267-273.

(5) Wiley, T. E.; Miller, W. R.; Miller, N. A.; Sension, R. J.; Lodowski, P.; Jaworska, M.; Kozlowski, P. M. *J. Phys. Chem. Lett.* **2016**, *7*, 143-147.

(6) Snellenburg, J. J.; Laptenok, S.; Seger, R.; Mullen, K. M.; van Stokkum, I. H. M. Glotaran: A Java-based graphical user interface for the R package TIMP. *Journal of Statistical Software [Online]* [Online Early Access]. DOI: 10.18637/jss.v049.i03. Published Online: 2012. http://dx.doi.org/10.18637/jss.v049.i03.

(7) Kas, J. J.; Jorissen, K.; Rehr, J. J. In *X-Ray Absorption and X-Ray Emission Spectroscopy*; John Wiley & Sons, Ltd: Chichester, UK., 2016, p 51-72.

(8) Brouder, C. *J. Phys. Condens. Matter* **1990**, *2*, 701-738.

(9) Lodowski, P.; Jaworska, M.; Andruniów, T.; Garabato, B. D.; Kozlowski, P. M. *Phys. Chem. Chem. Phys.* **2014**, *16*, 18675-18679.